

Slidegate Dithering Effects on Transient Flow and Mold Level Fluctuations

Rui Liu¹, Brian G. Thomas¹, Love Kalra², Tathagata Bhattacharya³, and Aloka Dasgupta²

¹Department of Mechanical Science and Engineering,
University of Illinois at Urbana-Champaign,
1206 W. Green Street, Urbana, IL, USA 61801
Phone: (217) 333-6919
Fax: (217) 244-6534
Email: bgthomas@illinois.edu

²ArcelorMittal No. 3 Steel Producing (Door 438)
3001 Dickey Road, East Chicago, IN 46312, USA
Phone – (219) 399-2259
Fax – (219) 391-2538
Email: love.kalra@ArcelorMittal.com

³ArcelorMittal Global R&D at East Chicago
3001 E Columbus Drive, East Chicago, IN 46312, USA
Phone – (219) 399-6453
Fax – (219) 399-3899
Email: tathagata.bhattacharya@arcelormittal.com

Keywords: slide-gate dithering, mold sloshing, free-surface tracking, dynamic mesh technique, mold level fluctuation

ABSTRACT

The effects of slide-gate dithering on surface flow behavior during continuous casting are investigated via mathematical modeling and plant trial measurements. A transient turbulent flow model with a new free surface tracking algorithm using a dynamic mesh was developed, validated, and applied to match different measured level-fluctuation histories. Simulation results explain the mechanism of large sloshing observed in a dithering trial when the dithering frequency matches the mold natural frequency. The associated flow-rate variations then amplify the velocity variations in the circulating fluid. Parametric studies reveal that mold level fluctuations increase with increasing casting speed, and dithering stroke.

INTRODUCTION

Slide-gate dithering has been implemented in continuous casting of steel to improve control of flow rate by oscillating the slide-gate back and forth at a particular stroke and frequency. The continuous motion prevents sticking and may also reduce clogging. However, slide-gate dithering also causes transient variations in fluid flow inside the submerged entry nozzle (SEN) as well as in the mold region [1]. This has a direct impact on mold level fluctuations, which is crucial to the quality of the final products. Mold level fluctuations are one of the most significant mechanisms responsible for mold slag entrainment and the formation of surface defects and other quality problems in the final product such as slivers [2].

Previous work on dithering has generally focused on measurement of mold level [3-5]. Control systems must be altered to maintain constant average flow rate and stable mold level, and special control algorithms have been developed to accomplish this [3-5]. Recently, dithering has been investigated using computational models [1], calculating mold level using a simple pressure method with a fixed wall condition imposed at the slag / steel interface. With a low frequency dithering practice (0.4 Hz) and a 1840-mm mold width, the periodic mold level change was found to be dominated by mass conservation of the liquid steel. Their predictions of mold level fluctuations using the pressure method were compared favorably with plant

measurements from the dithering trial. This method thus has been found to be reasonably accurate for relatively small surface waves. For larger waves, capable of causing sloshing, the effects of gravity need to be incorporated, so a free-surface tracking / capturing algorithm, such as the volume of fluid (VOF) method [6] has to be implemented in the model. In this work, models were developed, validated and combined together as a system to predict 3-D transient turbulent flow in the nozzle and mold region, together with argon gas effects using an efficient new free-surface tracking of this complicated flow system. In addition, a simple analytical model based on mass conservation of the liquid was developed and validated. The detailed mechanism of how mold flow activates the mold sloshing was revealed and parametric studies were conducted to study the effects of casting speed, mold width, and dithering stroke on mold level fluctuations.

PLANT MEASUREMENTS

During recent dithering trials conducted at ArcelorMittal Indiana Harbor 3SP, various slide-gate dithering conditions were investigated (dithering frequency and stroke) for different casting speeds and mold widths. The eddy current sensor recorded the mold level at the mold quarter point, and an example of the results is plotted in Figure 1. Large sloshing waves were observed in the mold with a 1840 mm (72.5 inch) slab width by mold operators at a dithering frequency of 0.9 Hz, which prompted switching to manual level control for safety. The gravity wave that caused this large amplitude sloshing in the mold has not been predicted in previous models [1].

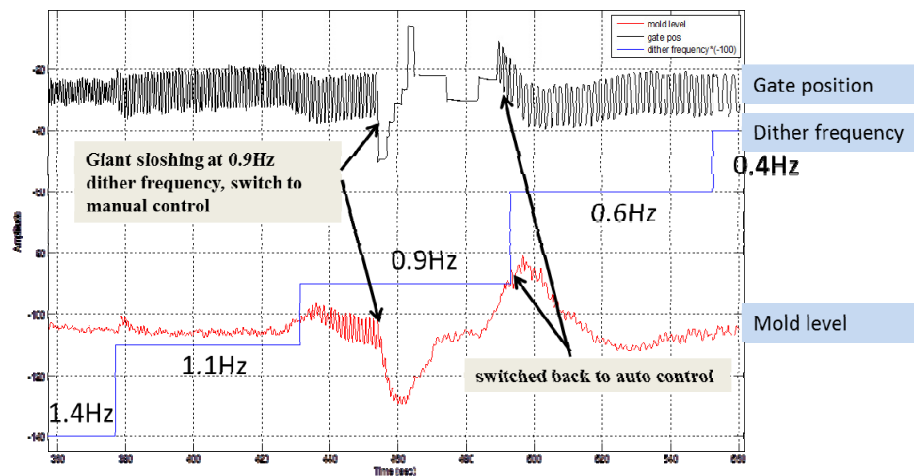


Figure 1. Dithering trials with mold level measurements in ArcelorMittal Indiana Harbor, 3SP

The effect of dithering frequency on mold level fluctuations is further plotted in Figure 2. Both the maximum and the root mean square of the measured mold level fluctuations are calculated and presented. For most frequencies (other than 0.9 Hz), the mold level fluctuations are affected only by the dithering stroke, and dithering frequency has little effect. However, when the dithering frequency was 0.9 Hz, (1840 mm width), both the *rms* and maximum mold level fluctuations jumped to about 4-5 times larger than those from all the other cases. These giant mold level fluctuations (over 10 mm from peak to valley) were identified to be caused by severe mold sloshing waves. The purpose of this paper is to create and apply computational and analytical models to investigate the effect of dithering on mold level fluctuations, including the prediction and understanding of the sloshing mechanism that causes the giant level fluctuations.

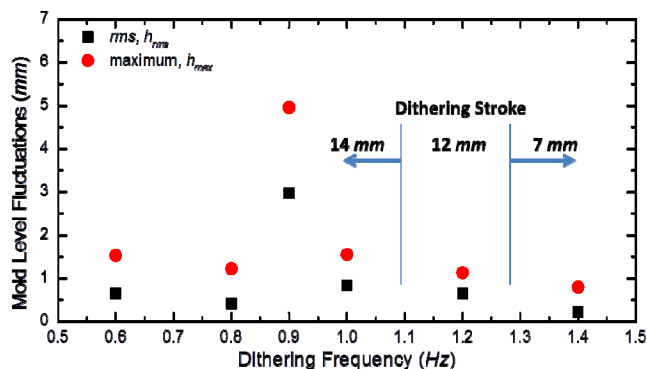


Figure 2. Influence of dithering frequency on mold level fluctuations

MOLD SLOSHING ESTIMATION

Sloshing in the mold resembles that in a rectangular tank, which has been well investigated by previous researchers [7-8]. The natural frequency for the tank sloshing problem is given by equation (1) below [7], and pictured in Figure 3.

$$f_{i,j}^2 = \frac{g}{4\pi} \sqrt{\left(\frac{i}{a}\right)^2 + \left(\frac{j}{b}\right)^2} \tanh \left[\pi h \sqrt{\left(\frac{i}{a}\right)^2 + \left(\frac{j}{b}\right)^2} \right] \quad (1)$$

where f (Hz) is the natural frequency,

i and j are sloshing mode indices along the x and y-axis respectively,

a , b and h , (m) are the tank dimensions in the x, y and z-directions respectively,

g is gravity acceleration (9.81 m/s^2).

The sloshing frequencies for different mold dimensions using equation (1) are plotted in Figure 4 below. Because the caster is deep, the \tanh term in equation (1) is about 1, so can be neglected. From Figure 4, for a slab width of 1840 mm, (72.5 inch), the first-mode, half-width from SEN to NF (0,1), or the second-mode, full-width from NF to NF (0,2), the sloshing frequency is 0.92 Hz in both cases, which is very close to the sloshing frequency observed in the plant. Thus, Figure 4 shows the mold width / dithering frequency combinations to avoid. Other specific frequencies to avoid are 1.17 Hz for a 1143-mm (45-inch) wide slab, 1.1 Hz for a 1270-mm (50-inch) wide slab, 1.0 Hz for a range of slab widths between 1524-mm (60-inch) and 1650-mm (65-inch).

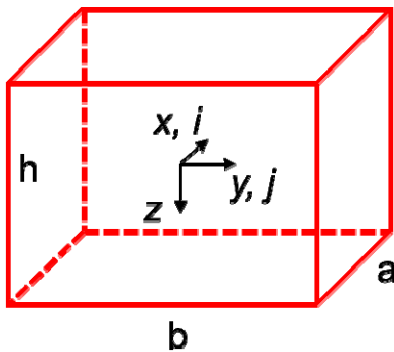


Figure 3. Schematic of sloshing mode indices

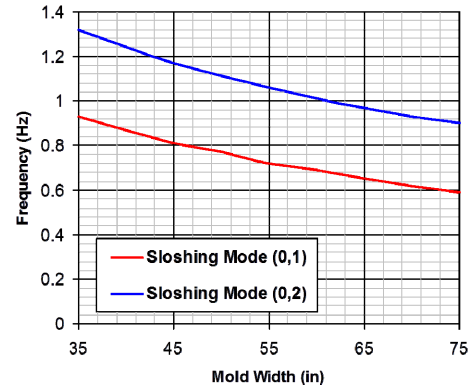


Figure 4. Mold natural frequency curves

MODEL DESCRIPTION AND VALIDATION

A system of models has been developed to handle each of the complex phenomena associated with the effect of slide-gate dithering on transient, turbulent, multiphase flow in the nozzle and mold and the associated mold level fluctuations, and is presented in Figure 5.

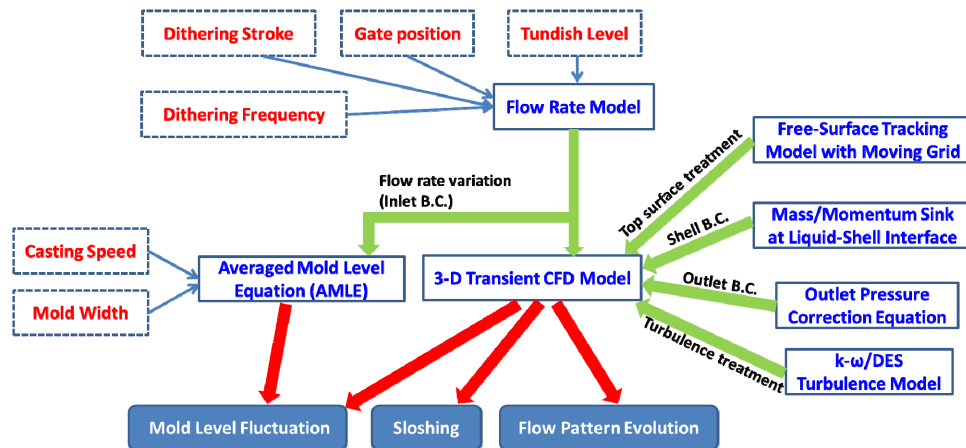


Figure 5. Model system for dithering process simulations

First, the liquid steel flow rate through the SEN is calculated based on the position of the slide-gate recorded during dithering by adapting a flow rate model from previous study [1]. Next, the 3-D flow pattern in the SEN and mold are calculated by solving the transient Navier-Stokes equations using the standard K-ε model for turbulence with the CFD package, FLUENT. In order to model the gravity waves, a new free-surface tracking algorithm with an adaptive dynamic mesh is employed to compute the motion of the mold top surface. A simple analytical model based on the liquid steel mass conservation was developed to calculate the average mold level change during the dithering process. All of these models were validated with experimental measurements, and then applied to investigate the transient flow pattern evolution and mold level fluctuations during slide-gate dithering.

Flow Rate Model

The liquid steel flow rate into the upper tundish nozzle (UTN) and submerged entry nozzle (SEN) varies with the slide-gate position during dithering. In previous work, [1] the flow rate through a water model was measured as a function of slide-gate opening position and found to match the following Bernoulli's equation (2) for a 90mm diameter SEN with 75-mm slide-gate bore. The parameter C in equation (2) below is the clogging factor, which is set to 0 in the current study. The match with measurements is shown in Figure 6.

$$Q_{SEN} = A_{eff} \sqrt{\frac{2g(H_1 + H_2)}{\left(\left(\frac{A_{SEN}}{A_{port}} - 1\right)^2 + f \frac{L_{SEN}}{D_{SEN}} + \left(\frac{1}{\mu} - 1\right)^2 \left(\frac{A_{SEN}}{A_{GAP}}\right)^2 + \left(\frac{A_{SG}}{A_{GAP}} - \frac{A_{GAP}}{A_{SG}}\right)^2 \left(\frac{A_{SEN}}{A_{SG}}\right)^2 + \left(\frac{A_{SEN}}{2A_{port}}\right)^2 + C\right)}} \quad (2)$$

where Q_{SEN} is the calculated fluid volumetric fluid flow rate in UTN / SEN,
 H_1 (m) is the distance between the tundish level and bottom of the tundish,
 H_2 (m) is the distance from UTN upper edge to the upper edge of SEN port exit,
 g is the gravitational acceleration (m/s^2),
 A_{SEN} (m^2) is the SEN inner cross-section area,
 A_{port} (m^2) is the area of the port exit projected to the liquid steel jet direction,
 f is the friction factor for turbulent flow in a circular pipe, with an estimated value of 0.075 from the Moody's chart,
 L_{SEN} (m) is the SEN length,
 D_{SEN} (m) is the SEN inner diameter, (90mm in water model; 80mm in caster)
 μ is the coefficient of contraction,
 A_{SG} (m^2) is the area of the slide gate when it is fully opened,
 A_{GAP} (m^2) is gap opening area projected in the casting direction, which depends on measured slide gate position

Note that fluid density does not appear in equation (2): this equation also describes liquid steel flow rate in the SEN. This model was used in this work to generate the boundary conditions at UTN inlet for both models of mold surface level.

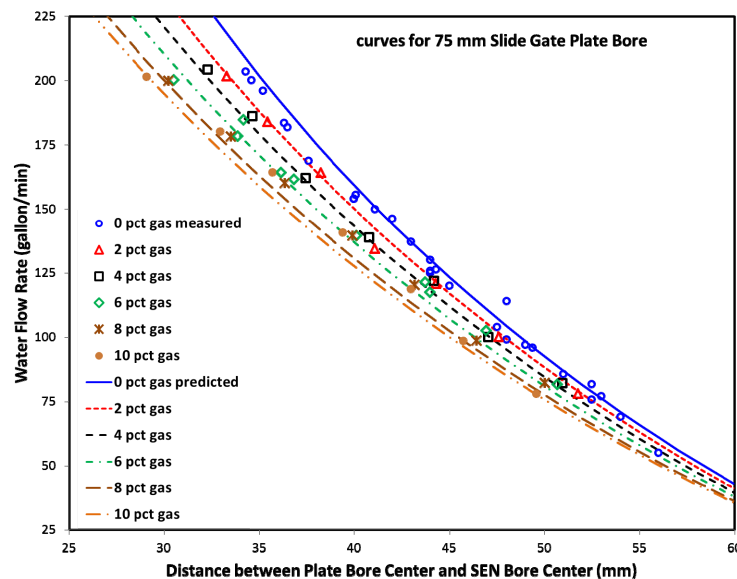


Figure 6. Comparison of flow rate model results with water model experiments data [1]

Free-Surface Tracking Model using Dynamic Mesh Technique

The volume of fluid (VOF) method [6] has been widely used in previous work to track free-surfaces. Because it involves solving a separate transport equation for phase volume fraction, it is difficult to apply both the VOF method and a separate two-phase flow model, such as the Eulerian-Eulerian method for bulk motion of the molten steel and argon gas, at the same time. It also requires a very fine mesh to achieve the accuracy in free surface movement that is needed for predicting mold level fluctuations.

To avoid these problems, a new method has been developed to calculate free surface motion, including gravity wave effects. It uses a free-surface tracking technique developed by Muzaferija and Peri'c [9] based on local fluid mass conservation. This simple method is accurate even if the mesh is coarse, and is compatible with two-phase flow modeling of the bulk liquid flow. A similar method, known as the SPINES method [10] in the commercial finite-element code, FIDAP, was successfully applied to simulate the slag-steel interface shape around a nail perimeter due to molten steel surface flow velocity [11]. The results were later validated with plant measurements [12], although the method had convergence problems. To overcome this problem, the dynamic mesh capability of ANSYS-FLUENT [13] for moving the mesh every iteration has been combined with a user defined function (UDF) of Muzaferija and Peri'c's free-surface method [9] to create a new free-surface tracking / dynamic mesh technique within ANSYS-FLUENT 14.0.

To validate the new surface-tracking / dynamic mesh method, a benchmark problem of 2-D small-amplitude sloshing in a tank [14] was calculated using the new model. The tank has 1.5m depth, 1.0 m width, and initial free-surface profile given by equation (3), including a 0.02 m perturbation as pictured in Figure 7. The fluid kinematic viscosity is $0.01 \text{ m}^2/\text{s}$ and gravitational acceleration is 1.0 m/s^2 . Two simulations were performed with a 25×40 coarse mesh and 200×80 fine mesh with constant time steps of 0.01 sec for the coarse mesh, and 0.002 sec for the fine mesh. An analytical solution of this small-amplitude sloshing problem is given [8] as follows.

$$h(x) = 1.5 + 0.01 \sin(\pi(0.5 - x)) \quad (3)$$

where h (m) is surface level,
 x (m) is the distance from left edge of tank.

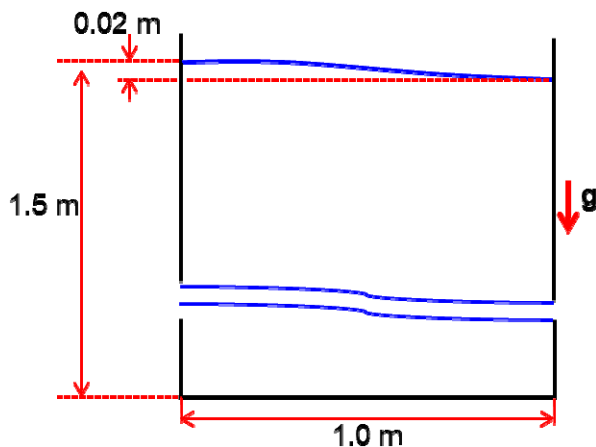


Figure 7. Schematic for small sloshing in a tank

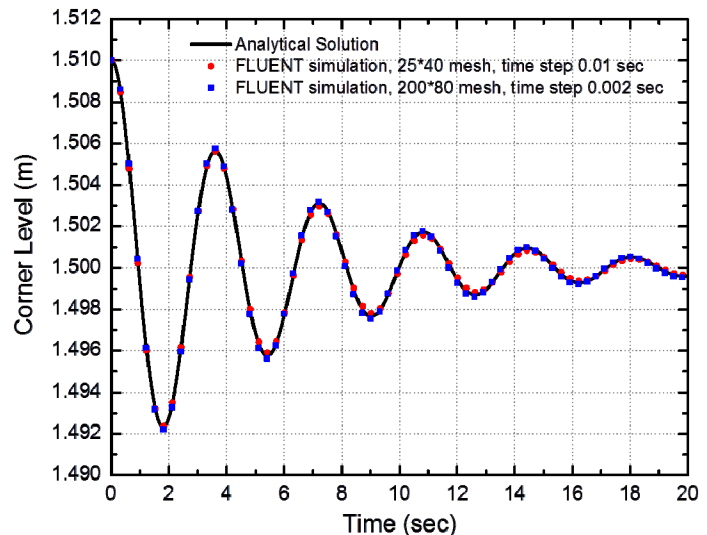


Figure 8. Validation of the free-surface tracking model

An excellent match between the computational-model and analytical results is found from the comparison in Figure 8. It is worth mentioning that even for a very coarse mesh of 25×40 , a close match between numerical and analytical solutions can still be obtained, even though the grid spacing is much larger than the maximum sloshing magnitude. It is also observed that the fluid viscosity gradually damps the sloshing, but the sloshing frequency remains the same as time progresses. Thus, the new free-surface tracking model developed in the current work is an ideal approach to model top-surface mold-level fluctuation behavior in continuous casting.

3-D Transient CFD model for SEN / mold flows

The computational model of transient turbulent flow is described in this section, including the governing equations, the geometry and mesh of the domain, and the boundary conditions.

Governing equations

The governing equations for current transient fluid flow model include the mass-conservation equation (4), and the momentum-conservation equation (5), which must consider the moving mesh velocity.

$$\nabla \cdot (\rho(\mathbf{v} - \mathbf{v}_g)) = 0 \quad (4)$$

$$\frac{\partial(\rho\mathbf{v})}{\partial t} + \nabla \cdot (\rho\mathbf{v}(\mathbf{v} - \mathbf{v}_g)) = -\nabla p + \nabla \cdot (\mu\nabla\mathbf{v}) + \rho\mathbf{g} \quad (5)$$

In equations (4) and (5), \mathbf{v}_g is the node velocity in the dynamic mesh region, which was defined in the upper (moving mesh) layer of the fluid bulk domain, and simply is 0 elsewhere in the domain. Further equations for conservation of the argon gas mass and momentum, and the two extra transport equations for the parameters in the $k-\omega$ turbulence model are given elsewhere [1,15]. Details of the DES model can be found in [16].

Computational domain geometry and mesh

Half of the full slide-gate, nozzle and mold region is taken as the computational domain, due to symmetry, as shown in Figure 9(a). The mold domain has been divided into two sub-domains, an upper 10-cell (100 mm) layer for the dynamic mesh region and a lower layer for the bulk of the fluid (2400 mm) with fixed mesh (shown in Figure 9(a)). This division of the fluid bulk is done for computational efficiency, as only the mesh near the meniscus must be smoothed to preserve mesh quality. To make the most coupled parts of model parallelizable for best computational efficiency, the upper layer of the mold bulk is assigned to a single processor, while the rest of the domain is split between 5 processors. Thus, slow mesh updating between processors is avoided in each iteration, and computational efficiency is better.

A mesh of 1 million hexahedral cells was adopted for all simulations, as shown in Figure 9(b)-(c). Close-ups are shown around the slide-gate region in Figure 9(b), and around the free surface region near the SEN and mold in Figure 9(c).

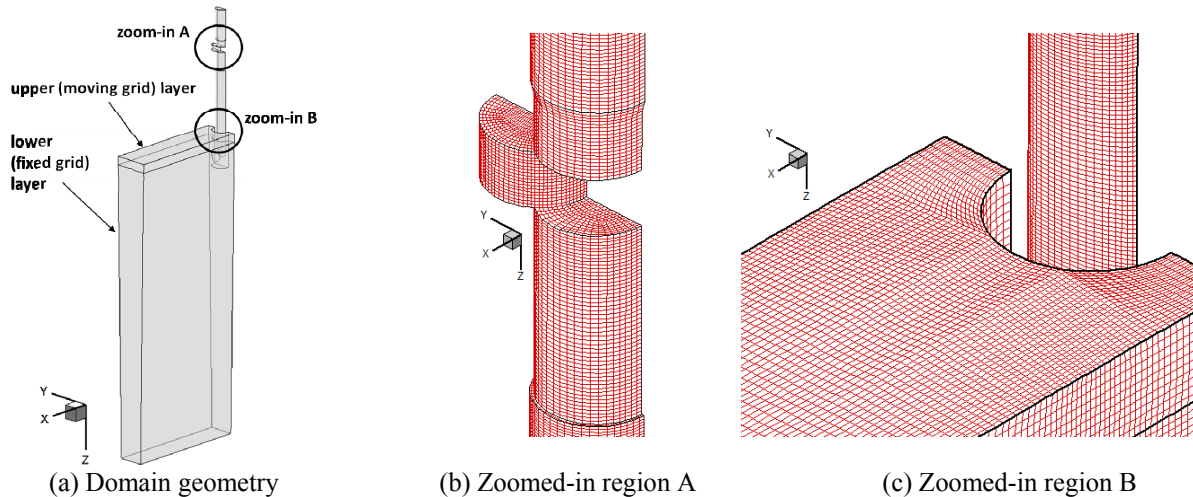


Figure 9. Domain geometry and mesh setup

Boundary conditions

The boundary conditions for the dithering process simulations include the UTN inlet for liquid steel, the mold top surface, solidified shell, and outlet from the domain bottom. For each of these boundaries, a special sub-model was applied, as detailed below.

UTN inlet B.C. with liquid steel flow rate history

Liquid steel flow rate from the flow-rate model is converted to a prescribed-velocity history boundary condition at the UTN inlet. Usually this velocity could be calculated from the casting speed. However, the dithering process causes periodic variations in flow rate/velocity due to the periodic change of slide-gate position. Thus, this flow rate history is calculated using equation (2).

Shell B.C. with mass/momentum sinks

Near the liquid-shell interface, liquid steel continuously solidifies into a solid shell, which moves downwards at the constant casting speed. The shape of the shell does not change with time, when viewed in an Eulerian frame of reference. Thus, in the current work, a moving-wall boundary condition (at the casting speed) is applied at the shell boundary. To account for liquid

steel exiting the domain across this wall, mass and momentum sinks are incorporated via a UDF. A detailed derivation of these sink terms is found in [17].

Domain top surface B.C.

Motion of the mold top surface is modeled with the free-surface tracking approach using the FVM dynamic mesh technique detailed in the previous section. The boundary conditions on the slag-steel interface (domain top surface) require no-penetration of fluid through the slag / steel interface (kinematic B.C.) and all forces in equilibrium at free surface (Dynamic B.C.). The kinematic boundary condition is given by equation (6), where \mathbf{v} is the fluid velocity and \mathbf{v}_s is the free surface velocity.

$$\left[(\mathbf{v} - \mathbf{v}_s) \cdot \mathbf{n} \right]_{fs} = 0 \quad (6)$$

At the mold top surface, a liquid flux layer that floats on the liquid steel surface adds a roughly constant pressure to the slag-steel interface. The thickness of the top liquid flux layer varies with position on the surface. Considering the unsteady nature of the slag-steel interface motion, it is assumed that the liquid flux and powder layers do not have enough time to re-distribute during the dithering cycle, so it is reasonable to assume a constant thickness (pressure) on top of liquid steel. Furthermore, the turbulence model is designed to filter (average) local instantaneous small-scale turbulent eddies, so the curvature of the domain top surface is small enough to neglect surface tension effects. With these assumptions, the dynamic boundary condition is given by equation (7):

$$p = p_0 + \rho_{flux} g h_{flux} + \mathbf{n} \cdot \mu \left[\nabla \mathbf{v} + (\nabla \mathbf{v})^T \right] \cdot \mathbf{n} \quad (7)$$

The pressure p_0 in the right-hand side of equation (7) is atmospheric pressure, (0.101MPa), ρ_{flux} is 3000 kg/m³, g is 9.81 m/s², and h_{flux} is the constant (20-mm) thickness of the flux and powder layers, and \mathbf{v} is the velocity vector at free surface. \mathbf{n} is the normal unit vector of the local free surface.

Domain outlet pressure B.C.

Hydraulic pressure of the liquid steel at the domain outlet is usually adopted for mold flow simulations with fixed wall boundaries at the top surface. When a pressure boundary condition such as equation (7) is applied at the domain top surface, however, a more accurate outlet boundary is needed. In this work, this pressure boundary condition is modified to ensure that the current liquid steel flow rate is matched at the domain outlet. The correction to the outlet boundary pressure is given by equation (8),

$$d\bar{p} = \rho \frac{\left(\frac{Q_T}{WT} \right)^2 - \left(\frac{Q_C}{WT} \right)^2}{2} \quad (8)$$

where Q_T is the target volumetric flow rate of liquid steel in the system,
 Q_C is the current volumetric flow rate at the domain outlet,
 W and T are the slab width and thickness at the domain bottom outlet.

This equation is based on Bernoulli's equation, as derived in [17]. This modification of boundary pressure is crucial to a successful dithering simulation, because the motion of the slag-steel interface can only be accurately computed if the outlet flow rate is correct and properly conserves mass in the entire system.

Model Validation with Plant Measurements

The entire 3-D multiphase computational model including the new free surface prediction method was validated by comparing with plant measurements with dithering. Simulations were performed for the conditions of Liu et al [1], which include dithering (14 mm stroke, 0.4 Hz frequency), 1.0 m/min casting speed, 1840 mm width, and 6% argon gas in hot condition. The predictions from the two different free-surface models are compared in Figure 10 with the mold level sensor measurements. As observed in Figure 10, both methods match reasonably well with the experiment measurements, and this new numerical model is again validated.

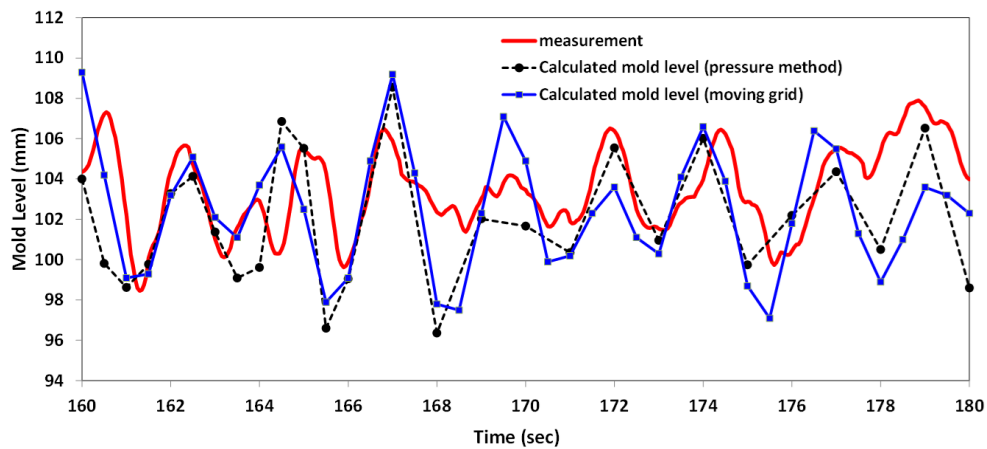


Figure 10. Free-surface model validation of mold level fluctuation with an argon-steel two-phase mold flow simulation

Model Validation with DES model

Before performing a simulation of transient behavior such as dithering, the CFD model is first run for ~ 10 sec (in physical time) until the flow is established. Instantaneous results using two different turbulence models, the $k-\omega$ model and the Detached Eddy Simulation (DES) model, are compared in this section. The $k-\omega$ model resembles the standard $k-\epsilon$ two-equation model for unsteady Reynold's averaged Navier-Stokes (U-RANS) simulation [15]. The DES performs Large Eddy Simulation (LES) in the fluid bulk region to capture the local instantaneous turbulent eddies, and adopts a RANS wall function close to the no-slip wall to resolve the details of the turbulent boundary layer fluctuations with less computational effort than LES [16].

The free surface and velocity results from these two models are compared in Figure 11 (a) and (b). The $k-\omega$ model generates the expected smoothed top surface profile, while DES gives an instantaneous surface shape. Both simulations give a lower surface level and higher surface velocity around the quarter mold region, while the top surface rises near the SEN and the narrow face, with a lower surface velocity.

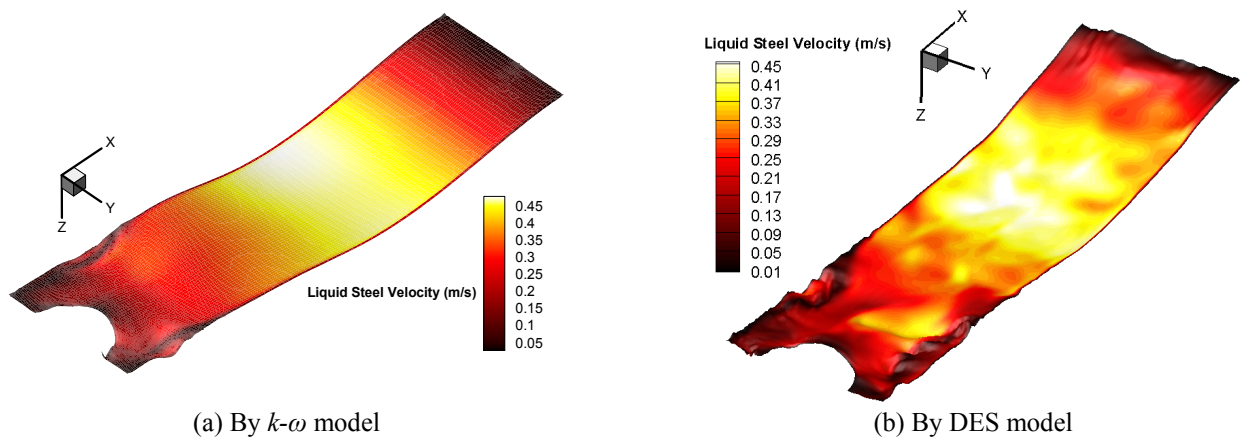
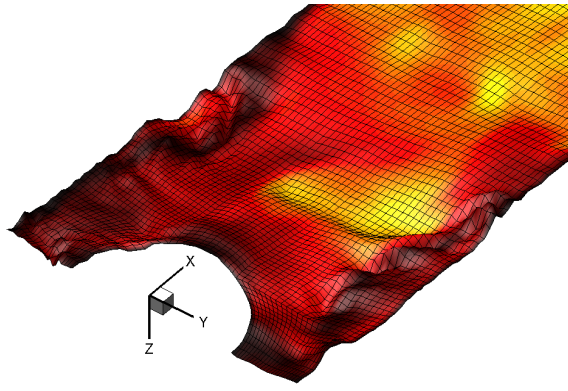
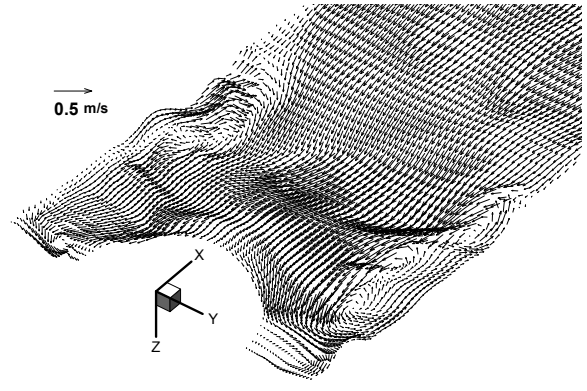


Figure 11. Comparison of simulated mold top surface morphologies by different turbulence models

Figure 12(a) shows the zoomed-in deformed shape of the mold top surface during constant casting speed without dithering, from the DES model. Note that the length scale in the vertical (z-) direction is stretched by 5 times, for easier visualization of the shape. Small vortices and wrinkles appear, especially near the SEN outer perimeter. The mold level rises close to the SEN, due to the impingement of the liquid steel stream flowing towards the SEN. Velocity vectors along the free surface are plotted in Figure 12(b). Recirculation regions are observed near both sides of the SEN, which cause dimples (depressions) to form on the free surface.



(a) Free surface morphology with mesh deformation



(b) Top surface liquid steel velocity close to SEN

Figure 12. Zoomed-in of free surface close to SEN calculated using DES (length magnified by 5 times along z-axis)

Averaged Mold Level Equation (AMLE)

Changes of the average mold level can be derived by performing a mass balance on the steel flow-rate history averaged over the cross-sectional area of the entire computational domain. Balancing the flow rate variations through the SEN with changes in average surface level in the mold leads to equation (9).

$$V_l \left(A_l - \frac{\pi}{4} D_o^2 \right) + V_c A_l = Q_{SEN} \quad (9)$$

where V_l (m/s) is the average vertical velocity of the liquid steel surface level in the mold,
 A_l (m²) is the slab cross-section area at meniscus,
 D_o (m) is the outer diameter of SEN,
 V_c (m/s) is the casting speed.

Integrating the velocity V_l in equation (9) gives the mold level $h(t)$ in equation (10), integrated numerically to equation (11) below:

$$h(t) = \int_{t_0}^t \left(\frac{Q_{SEN}}{\alpha_A A_l} - \frac{V_c}{\alpha_A} \right) dt' + h_0 = \frac{1}{\alpha_A A_l} \int_{t_0}^t Q_{SEN} dt' - \frac{1}{\alpha_A} \int_{t_0}^t V_c dt' + h_0, \quad \alpha_A = 1 - \frac{\pi D_o^2}{4WT} \quad (10)$$

$$h_n = \frac{1}{\alpha_A A_l} \sum_{i=0}^n Q_{SEN}(t_i) \Delta t - \frac{1}{\alpha_A} V_c (t_n - t_0) + h_0 \quad (11)$$

where t_n (sec) is the time at time step n
 h_n (mm) is the average mold level at time t_n , relative to h_0 at t_0 measured at the start of the time interval
 Q_{SEN} (m³/s) is volumetric flow rate from equation (2), based on the measured slide-gate position
 W (m) is the mold width,
 T (m) is the mold thickness.

Since the averaged mold level position is an integral of the SEN liquid steel flow rate over time, a sudden change of the flow rate takes time to affect the mold level. Similar approaches used to estimate mold level fluctuations can also be found in previous studies where researchers used the predicted mold level fluctuations to calibrate their control algorithms [3, 5]. To quantify the fluctuations in mold level, equation (12) defines the standard deviation or “root mean square” (rms) of the mold level fluctuation relative to the mean level (\bar{h}). Larger h_{rms} indicates higher chances of quality problems:

$$h_{rms} = \sqrt{\overline{h'^2}} = \sqrt{\frac{\sum_{i=1}^N (h_i - \bar{h})^2}{N}} \quad (12)$$

where h (mm) is mold level; and \bar{h} is time average
 N is the total number of sampling points (~1000, taken over time interval of 10 sec).

To validate this model, it is first applied to predict average mold level fluctuation results for cases with plant measurements. The measured and predicted mold level fluctuations are compared in Figure 13.

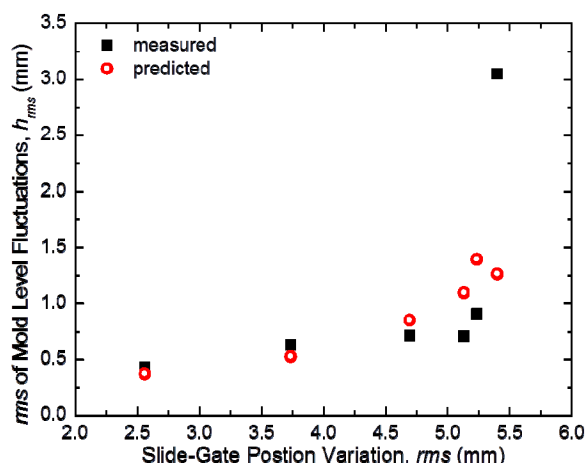


Figure 13. Comparison between measured and predicted mold level fluctuations

In most of the cases, the predicted mold level fluctuations reasonably match the measurements. However, in the case with a 5.5 mm slide-gate position variation, a huge deviation appears. This is the case where severe mold sloshing was observed. In this case, the averaged mold level fluctuations are caused by gravity waves, so the prediction based on a mass balance on the flow rate cannot reflect the real slag-steel interface behavior. Thus, the AMLE model is accurate, unless giant sloshing occurs.

RESULTS AND DISCUSSION

This section presents the transient flow pattern and evolution of the slag-steel interface for the dithering process conditions that caused mold sloshing. The predicted mold level fluctuations are compared with plant measurements. A parametric study is then conducted to investigate the average mold level fluctuations during typical dithering processes. The mold dimensions for this study are 1840 mm width and 254 mm thickness. The SEN has 80mm inner bore diameter, roof-type bottom, and 80 mm diameter ports with a downward angle of 15 deg., 143 mm submergence depth, and 75 mm slide-gate plate diameter. These conditions are consistent with those used to generate the flow rate curves in Figure 6. A total flow rate of 1 SLPM argon was injected into the UTN, corresponding to about 1% gas volume fraction in hot condition. This is small enough that single phase flow was assumed in the current simulation.

Simulation results of the transient flow pattern evolution for the mold sloshing case with 0.9 Hz dithering frequency and 14 mm dithering stroke, and 1.0 m/min casting speed are shown in Figure 14 (a)-(e). Approximately five dithering cycles were simulated (starting from 0 sec), and the cycle from 3.0 sec to 4.1 sec is presented in Figure 14 and 15. At time 3.0 sec at the start of a dithering cycle, the strength of the liquid steel jet starts to increase. The mold top surface level is higher close to the SEN, and lower at the narrow face. At time 3.3 sec, the jet grows stronger, and the recirculation velocity around the upper roll is accelerated. During this time, the mold surface level near the SEN decreases, while the surface level at mold narrow face increases. The slag-steel interface is relatively flat by this time. At time 3.6 sec, the established jet starts to decrease in strength, due to the upstream closing of the slide-gate. At this moment, the surface level at mold narrow face reaches its peak. At time 3.8 sec, the jet is weakest, and the mold surface level near the SEN keeps increasing, while the level at mold narrow face continues to decrease. When the time reaches 4.1 sec, the surface level at the SEN has risen to its highest point, and begins to drop, while the level at the narrow face starts to increase from its lowest point. At the same time, the liquid steel jet strength starts to increase, and the next dithering cycle begins.

Throughout each dithering cycle, the liquid steel jet leads a wobbling path towards the mold narrow face due to the flow rate variation, and the flow pattern in mold region remains double-roll. The duration of this large scale eddy is long enough that the change of inlet liquid steel flow rate does not alter the flow pattern. The recirculation velocity in the upper roll is accelerated and slowed down periodically. When the dithering frequency matches the mold natural frequency, as in this simulation, the increase of the jet strength accelerates the rising velocity of the mold surface level at narrow face. In this manner, the kinetic energy increase from the jet outweighs the energy dissipated by the viscous effects. Thus mold sloshing gets energized and magnified in every dithering cycle.

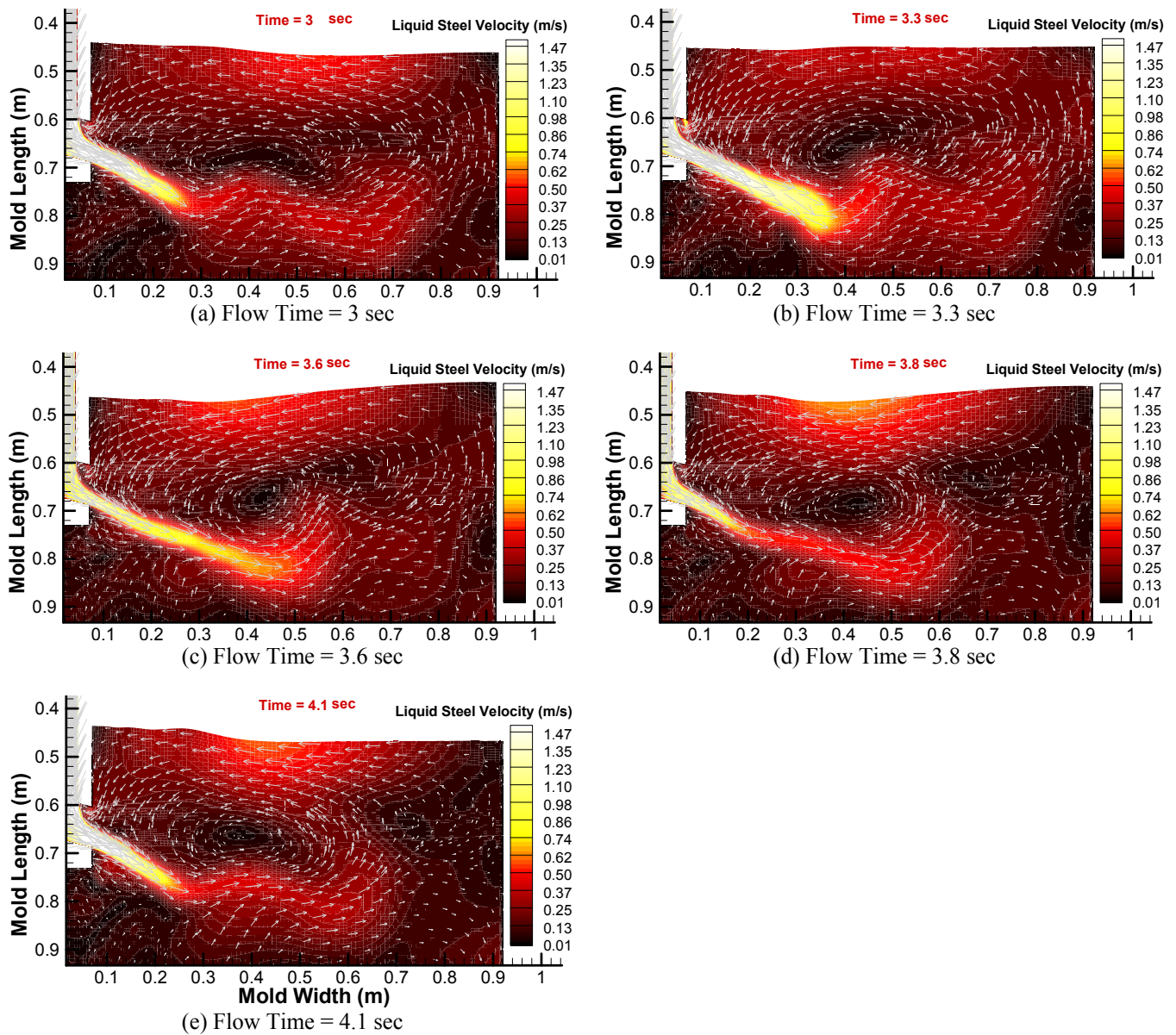


Figure 14. Transient liquid steel flow pattern evolution during one dithering cycle for the mold sloshing case

The 3-D motion of the mold top surface is shown in Figure 15 (a)-(e), where the contours indicate the local level. Dark regions indicate high surface levels, while red regions have lower levels. From time 3.0 sec to 3.3 sec, surface level drops near the SEN, and increases near the narrow face. At time 3.3 sec, the surface levels are almost even. Then level at the narrow face starts increasing, from the increased momentum of the liquid steel jet flowing up the narrow face. At time 3.6 sec, surface level reached its maximum at the narrow face. For the next 0.5 sec, a ~35mm-high wave flows across the top surface towards the SEN, finally producing a maximum surface level at the SEN at time 4.1 sec. This time coincides with the beginning of the next dithering cycle, which causes the process to repeat in an amplified manner during the next dithering cycle.

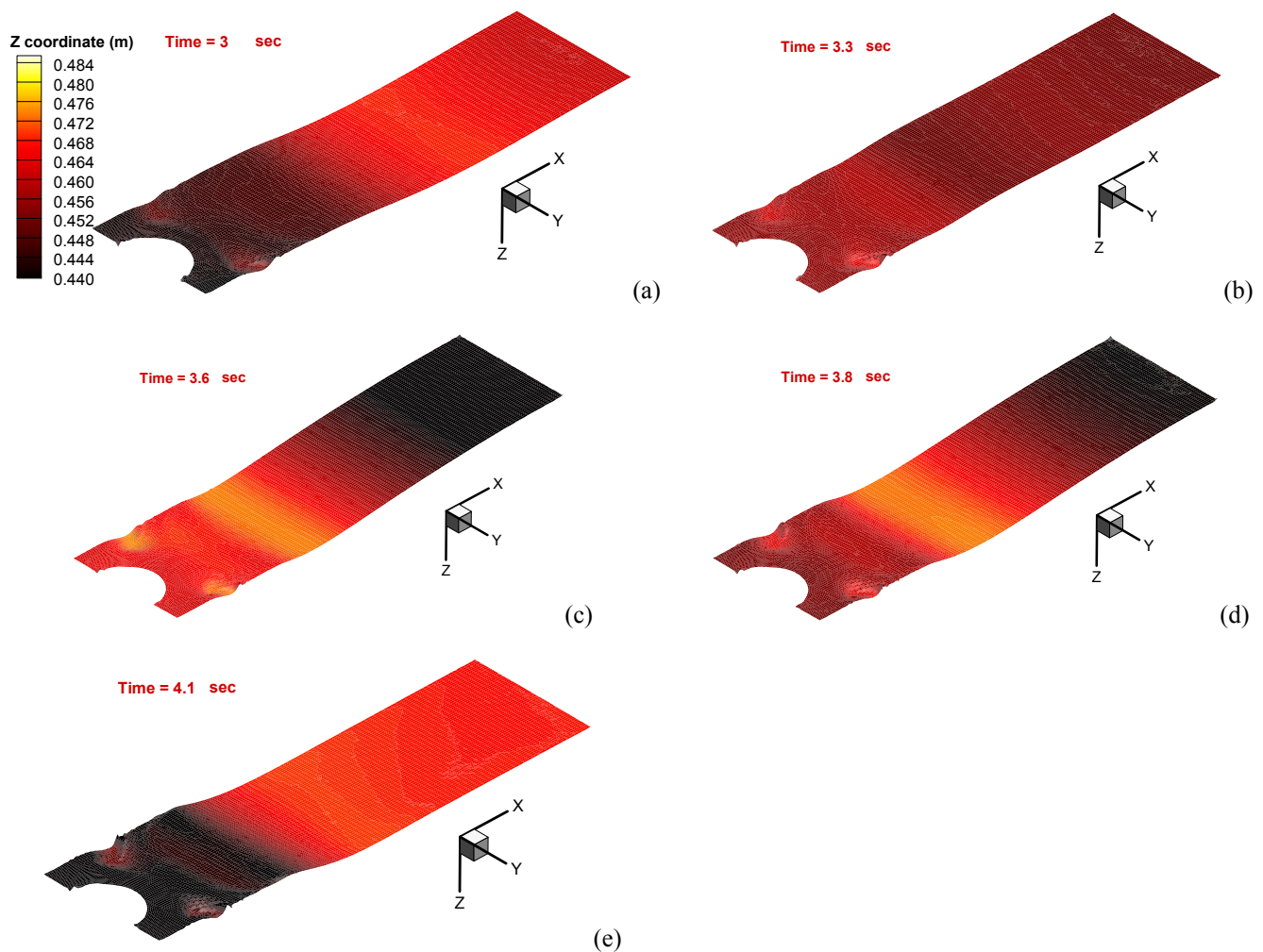


Figure 15. Mold top surface behavior during one dithering cycle

Parametric Studies

For dithering practices which do not activate the gravity-wave sloshing mechanism, mass conservation dominates the mold level fluctuations, as discussed previously [1]. Thus, parametric studies using the AMLE model were conducted to investigate the effects of casting speed and dithering stroke on the flow rate variations, and the mold level fluctuations, for a 1840-mm mold width. The flow-rate variations are calculated using equation 2 and presented in Figure 16(a). The mold level variations (*rms*) are calculated with equations 9-12 and shown in Figure 16(b). Note that the actual peak-to-valley mold level fluctuations are around 3 times of the mold level *rms* values calculated, as shown on the right axis in Figure 16(b). Five dithering strokes were modeled, 6, 8, 10, 12, and 14 mm, at three different casting speeds, 0.6, 1.0, and 1.4 m/min, (25, 40 and 55 inches per min).

Effects of Dithering Stroke

The effects of dithering stroke are shown in Figure 16 for different casting speeds. Liquid steel flow rate changes during dithering according to the dithering stroke. This causes the average mold levels to vary, while casting speed is constant. Increasing dithering stroke increases these flow-rate variations, which in turn increases the mold level fluctuations. Specifically, increasing dithering stroke from 6 mm to 14 mm increases flow rate variations by ~140 percent, causing level fluctuations to increase from ~0.25 mm to ~0.55 mm (*rms*) for low (0.6 m/min) casting speed, from ~0.3 mm to ~0.7 mm for medium (1.0 m/min) casting speed, and from ~0.35 mm to ~0.85 mm for high (1.4 m/min) casting speed.

Effects of Casting Speed

The effects of casting speed are shown in Figure 16 for different dithering strokes. As casting speed increases, the flow rate variations through the UTN increase as well. At lower casting speeds, the *rms* of mold level fluctuation is less than 0.7 mm, even with a high dithering stroke. When casting speed increases to 1.4 m/min, the *rms* of mold level fluctuation increases to ~0.8 mm for higher dithering strokes. The increase of mold level fluctuation (*rms*) is almost uniform when casting speed increases from 0.6 m/min to 1.0 m/min and from 1.0 to 1.4 m/min, for each of the dithering strokes. Specifically, average

mold fluctuations increase from ~ 0.7 mm to ~ 0.85 mm (rms) when increasing steady-state casting speed from 1.0 to 1.4 m/min (40 to 55 ipm), with a 14 mm dithering stroke.

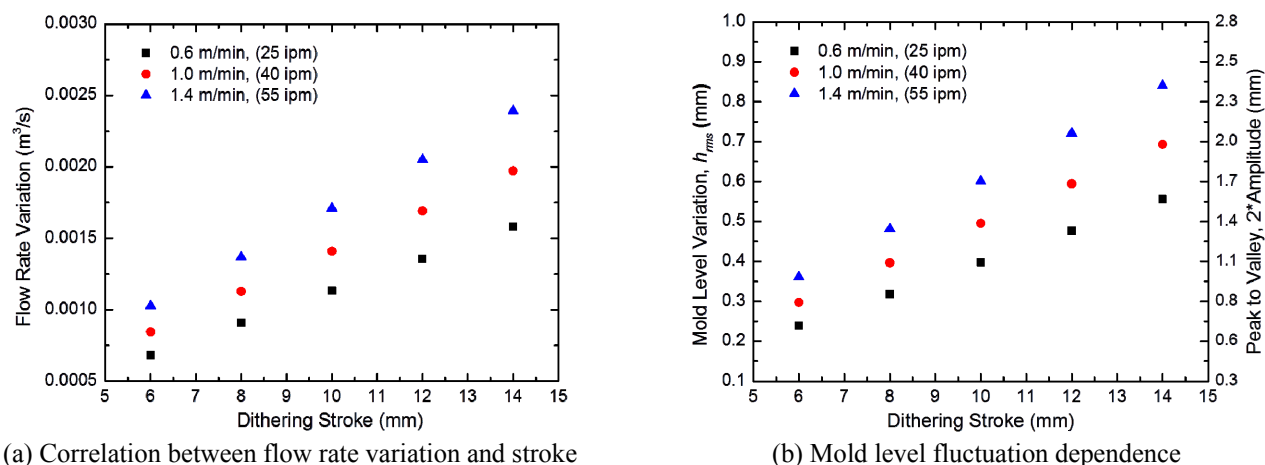


Figure 16. Effects of dithering stroke and casting speed on flow rate variation and mold level fluctuation

CONCLUSIONS

This work applies plant measurements and computational models to investigate the effect of slide-gate dithering on mold level fluctuations. Two different systems of models has been developed, validated separately and applied to capture the different physics occurring in this complicated real-world problem. Both a complex 3-D transient turbulent flow CFD model and a simple analytical model have been constructed to investigate the transient variations of flow pattern change, evolution of the slag-steel interface and average mold level fluctuations during the dithering of slide-gate for different operating conditions. A novel free-surface tracking model with a dynamic mesh technique was created utilizing the dynamic mesh feature of the commercial FVM CFD package ANSYS-FLUENT. From the results of both models, the following conclusions can be drawn:

1. The new free-surface tracking methodology was proven to be a promising approach to model both transient and steady state behavior of the slag-steel interface in terms of accuracy, computational efficiency and applicability to complex multiphase flow problems including severe sloshing;
2. Severe mold sloshing occurs when the dithering frequency matches the natural frequency of the mold, which is determined only by the mold dimensions;
3. The critical sloshing frequency is 0.9Hz for the 1840mm mold width studied here and decreases with increasing width;
4. The mechanism of sloshing and its detailed behavior is revealed by the simulation results, where the gravity wave periodically is energized by the increase of liquid steel jet momentum during the dithering cycle, resulting in the magnification of surface waves and mold level fluctuations;
5. The average mold level fluctuation can be calculated accurately using a simple analytical model developed in this work, as long as there is no severe sloshing;
6. Increasing casting speed during dithering increases the magnitude of the mold level fluctuations. Specifically, average mold level fluctuations increase from ~ 0.7 to ~ 0.9 mm (rms) or ~ 2.0 to ~ 2.4 mm (peak to valley) when increasing steady-state casting speed from 1.0 to 1.4 m/min (40 to 55 ipm), with a 14 mm dithering stroke. Thus, casting speed should be restricted when casting wide slabs (eg. 1840 mm or 72.5 inch), especially with high dithering stroke;
7. Increasing dithering stroke also increases the mold level fluctuations. Specifically, average mold level fluctuations increase from ~ 0.3 mm to ~ 0.7 mm (rms), or ~ 0.8 mm to ~ 2.0 mm (peak to valley) when dithering stroke changes from 6 mm to 14 mm, for the casting speed of 1.0 m/min (40 ipm), but ~ 0.4 to ~ 0.8 mm (rms) or ~ 1.0 to ~ 2.4 mm (peak to valley) for the casting speed of 1.4 m/min (50 ipm). Thus, dithering strokes larger than 12 mm should be avoided for casting speeds above 1.0 m/min (40 ipm) for wide slabs.

ACKNOWLEDGEMENTS

The authors thank the members of the Continuous Casting Consortium at the University of Illinois at Urbana-Champaign and the National Science Foundation (Grant CMMI-11-30882) for support of this research, and we want to thank Hongbin Yin, Kai Zheng and Bill Umlauf at ArcelorMittal Global R&D in East Chicago for providing the mold level measurement data.

REFERENCES

1. R. Liu, B.G. Thomas, B. Forman and H. Yin, "Transient turbulent flow simulation with water model validation and application to slide gate dithering", *AISTech Iron Steel Technol. Conf. Proc.*, 2012, Atlanta, GA, pp 1317.
2. L.C. Hibbeler, R. Liu and B.G. Thomas, "Review of Mold Flux Entrainment Mechanisms and Model Investigation of Entrainment by Shear-Layer Instability", *7th ECCO*, Düsseldorf, Germany, 2011.
3. S.F. Graebe, G.C. Goodwin and G. Elsley, "Control Design and Implementation in Continuous Steel Casting", *IEEE Control Systems Magazine*, 1995, **15**(8), pp 64.
4. R. de Keyser, "Improved Mould-Level Control in a Continuous Steel Casting Line", *Control Engineering Practice*, 1997, **5**(2), pp 231.
5. Q. Liu and W. Wang, "A Mold Level Mechanism Model in Continuous Casting with Application to Suppression of Limit Cycle", *ACTA AUTOMATICA SINICA*, 2002, **28**(3), pp 156.
6. C.W. Hirt and B.D. Nichols, "Volume of Fluid (VOF) Method for the Dynamics of Free Boundaries", *Journal of Computational Physics*, 1981, **39**, pp 201.
7. H. Lamb, *Hydrodynamics*, Dover Publication, 6th Edition, 1932.
8. A. Prosperetti, "Motion of Two Superposed Viscous Fluids", *Physics of Fluids*, 1981, **24**(7), pp 1217.
9. S. Muzaferija and M. Perić, "Computation of Free-Surface Flows using the Finite-Volume Method and Moving Grids", *Numerical Heat Transfer, Part B: Fundamentals*, 1997, **32**(4), pp 369.
10. M.S. Engelman, *FIDAP Theoretical Manual*, Fluent, Inc., 2001.
11. B. Rietow and B.G. Thomas, "Using Nail Board Experiments to Quantify Surface Velocity in the CC Mold", *AISTech Iron Steel Technol. Conf. Proc.*, 2008, Pittsburgh, PA.
12. R. Liu, J. Sengupta, D. Crosbie, S. Chung, M. Trinh and B.G. Thomas, "Measurement of Molten Steel Surface Velocity with SVC and Nail Dipping during Continuous Casting Process", *TMS Annual Meeting*, 2011, pp. 51.
13. Fluent ANSYS Inc., *User Manual*, 2011.
14. B. Ramaswamy and M. Kawahara, "Arbitrary Lagrangian–Eulerian Finite Element Method for Unsteady Convective Incompressible Viscous Free Surface Flow", *Int. J. Numer. Meth. Fluids*, 1987, **7**, pp 1053.
15. F.R. Menter, "Two-Equation Eddy-Viscosity Turbulence Models for Engineering Applications", *AIAA Journal*, 1994, **32**(8), pp 1598.
16. P.R. Spalart, W.H. Jou, M. Strelets and S.R. Allmaras, "Comments on the Feasibility of LES for Wings and on the Hybrid RANS/LES Approach", *Proc. of the 1st AFOSR Int. Conf. on DNS/LES*, Arlington, TX, 1997.
17. R. Liu and B.G. Thomas, "Slide-gate Dithering Effects on Transient Flow and Mold Level Fluctuations", *Continuous Casting Consortium Report*, Urbana, IL, 2012.